Nonconventional screening of Coulomb interaction in hexagonal boron nitride nanoribbons

A. Montaghemi,[1] H. Hadipour,[2,*] F. Bagherpour,[2] A. Yazdani,[1,†] and S. Mahdavifar[2]
[1]*Department of Physics, University of Tarbiat Modares, 14115-111 Tehran, Iran*
[2]*Department of Physics, University of Guilan, 41335-1914 Rasht, Iran*

(Received 1 January 2020; accepted 11 February 2020; published 24 February 2020)

Strong excitonic effects is a very subtle issue in pristine hexagonal boron nitride (h-BN) and h-BN nanoribbons (h-BNNRs) due to large band gaps and reduced dimensionality. One of the reasons for such a large exciton binding energy (as large as 2.5 eV) is weak dielectric screening. Employing first-principles calculations in conjunction with the constrained random-phase approximation, we determine the strength of the Coulomb matrix elements for pristine h-BN and h-BNNRs with armchair and zigzag edges. Due to the nonconventional screening, the calculated off-site U parameters for passivated h-BNNRs turn out to be rather sizable. Coulomb interaction is weakly screened at short distances and antiscreened at intermediate distances. Transition from screening to antiscreening takes place at a distance as low as 8 Å in narrow passivated h-BNNR. The critical distance for the onset of antiscreening in hydrogen-terminated h-BNNRs is longer than in zero-dimensional molecules and clusters, but shorter than in graphene nanoribbons and carbon nanotubes. With increasing the width of the passivated h-BNNRs from the critical point about 12.6 Å, the antiscreening effect is not observed. For completeness, on-site and long-range Coulomb interactions for metallic nonpassivated zigzag h-BNNRs are also reported.

DOI: 10.1103/PhysRevB.101.075427

I. INTRODUCTION

Two-dimensional (2D) systems such as graphene [1,2] have become one of the most studied classes of materials during the last decade. Graphene is not magnetic and has no band gap, which makes it difficult to use in electronic and spintronic applications. Several methods have been developed to turn graphene into a semiconductor and also to introduce magnetism [3–9]. Most of these systematic approaches are not able to be precisely controlled. It is very desirable to find 2D materials that are magnetic or have a band gap in the pristine form. Boron and nitrogen atoms with strong covalent bonds in a hexagonal lattice, also called h-BN, is an insulator with an indirect band gap of about 5.0 eV [10–23]. The electronic and magnetic properties of h-BN nanoribbons (h-BNNRs) depend on their edge and width. Bare zigzag h-BNNRs (Zh-BNNRs) are magnetic metals [24], while hydrogen-passivated structures (Zh-BNNRs:H) are semiconductors with a band gap of 4.5 eV that decreases linearly with increasing ribbon width [25–27]. Both bare armchair h-BNNRs (Ah-BNNRs) and hydrogen-passivated armchair h-BNNRs (Ah-BNNRs:H) are semiconductors. For example, the band gap of Ah-BNNR:H of 6.3 Å width is about 4.5 eV [28] in the generalized gradient approximation (GGA).

Tightly bound excitons with binding energies of about 2.5 eV were observed experimentally in 2D h-BN [16,22,29]. This is larger than the corresponding binding energy in carbon-based materials and bulk semiconductors and is in good agreement with *ab initio* calculations [30]. It is worth noting that the formation of tightly bound excitons in 2D h-BN reveals a significantly reduced and nonlocal dielectric screening of the Coulomb interaction. Furthermore, the incorporation of electron-electron correlation effects within the GW approximation gives rise to the large band gap of 7 eV in Ah-BNNR:H, which is significantly larger than the band gap predicted by the GGA approximation [31]. Such a significant many-body GW correction to the band gap is associated with large Coulomb matrix elements. Also, the exciton binding energy for h-BNNRs:H is between 2.1 and 2.4 eV [32,33], which is higher than the equivalent graphene nanoribbons (GNRs) [34]. Moreover, the reduced dimensionality gives rise to a nonconventional screening of the Coulomb interaction in low-dimensional and finite-size insulators; that is, it is screened at short distances and antiscreened at intermediate distances [35–39]. Such a nonconventional screening of the Coulomb interactions occurs in GNRs [39,40] and semiconducting carbon nanotubes [36]. One of the consequences of a nonconventional screening is the large exciton binding energy (as large as 1.5 eV) in GNRs [34,41–45].

In the case of metallic h-BNNR with a zigzag edge, magnetism is a controversial issue and Coulomb interactions play a crucial role to describe the origin of ferromagnetic ordering. Generally, low-dimensional materials have a lower continuity of the density of states and, consequently, have less bandwidth than the bulk. As a result, the ratio of effective Coulomb interaction U to bandwidth W_b is increased, and the strength of the correlation U/W_b becomes great. One of the consequences of a moderate correlation $U/W_b \sim 1$ is inducing magnetism in the carbon-based materials [39,46,47].

The formation of tightly bound excitons in semiconducting Ah-BNNR and the existence of ferromagnetism in metallic Zh-BNNR motivate us to evaluate the *ab initio* Coulomb

*hanifhadipour@gmail.com
†yazdania@modares.ac.ir

interaction parameters in 2D h-BN and h-BNNR for different widths. The effective Coulomb interaction between localized electrons plays an important role in constructing a generic second-quantized Hamiltonian for BN materials and gives us useful information for describing the reason behind electronic and magnetic ordering.

In this paper, we study the screening of on-site and long-range Coulomb interaction between p_z electrons in passivated h-BNNRs and sp^3 electrons in bare h-BNNRs by employing *ab initio* calculations in conjunction with the constrained random-phase approximation [48–50] (cRPA) within the full-potential linearized augmented plane-wave (FLAPW) method. Due to the existence of similarities between h-BN and graphene, we compare our results with the recent study of the graphene nanoribbons [39]. Our results show the Hubbard U parameters for passivated h-BNNR:H with different width, slightly smaller than the ones in pristine h-BN. Also, screening in Zh-BNNR:H is stronger than that in Ah-BNNR:H. Due to the nonconventional screening, the transition from screening to antiscreening takes place at a distance as low as 8 Å in narrow passivated h-BNNR. We found that the antiscreening in h-BNNRs occurs in a shorter distance than observed in GNRs, but longer than in zero-dimensional molecules and clusters. In addition, there is a critical width such that if the nanoribbon width is larger than the critical width, the antiscreening effect is not observed.

II. COMPUTATIONAL METHOD

For the investigation of the hydrogen-passivated h-BNNR with armchair (N_a-Ah-BNNR:H) and zigzag edge (N_z-Zh-BNNR:H), we use conventional orthorhombic unit cells to simulate these systems, in which N_a is the number of dimer lines across the ribbon width and N_z is the zigzag chain across the ribbon. For comparison, bare Zh-BNNR and pristine 2D h-BN are also considered. In the armchair group, we consider $N_a = 2$ (2-Ah-BNNR:H) to $N_a = 11$ (11-Ah-BNNR:H) passivated nanoribbons. In the case of the zigzag group, passivated nanoribbons with $N_z = 3$ (3-Zh-BNNR:H) to $N_z = 9$ (9-Zh-BNNR:H) and $N_z = 7$ nonpassivated nanoribbon (7-Zh-BNNR) are considered. Figure 1 shows some of these nanoribbons. The unit cells are separated from them by 20 Å in both edge-to-edge and layer-to-layer directions. This vacuum separation is enough to ensure there is no interaction between the ribbon and its periodic images. Also, all atomic positions and lattice constants are relaxed, so the forces on each atom are converged until 0.02 eV/Å. A plane-wave basis set with 190 Rydberg cutoff energy has been used. For density functional theory (DFT) calculations, we use the FLAPW method as implemented in the FLEUR code [51] within the generalized gradient approximation parameterized by Perdew, Burke, and Ernzerhof (PBE) [52] for the exchange-correlation energy functional. Dense $24 \times 1 \times 1$ and $24 \times 24 \times 1$ k-point grids are used for unit cells of h-BNNRs and pristine h-BN, respectively. A linear momentum cutoff of $G_{\max} = 4.5$ bohr^{-1} is chosen for the plane waves. The SPEX code [53] uses DFT results to determine the strength of the partially (fully) screened effective Coulomb Interaction $U(W)$ between localized electrons from the first-principles cRPA method [48].

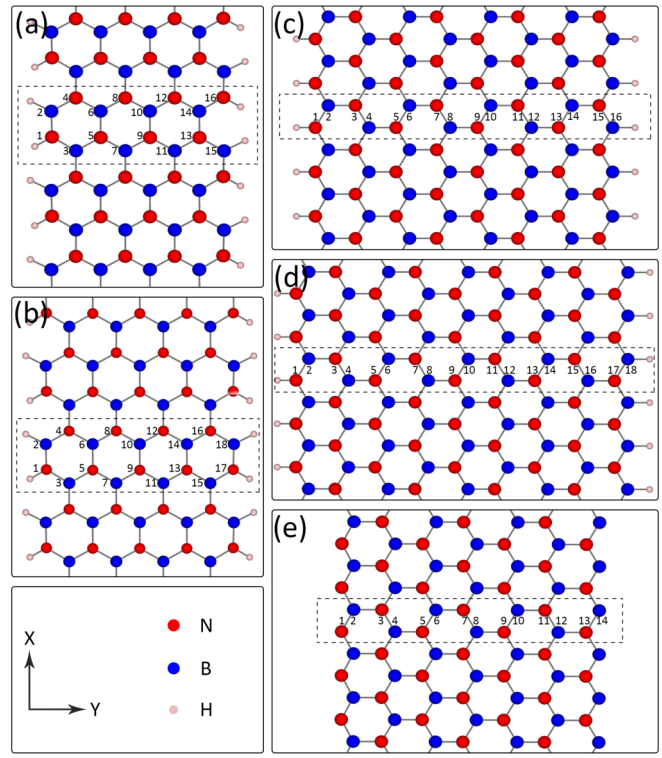

FIG. 1. h-BN nanoribbons with two types of edges: (a) $N_a = 8$ (8-Ah-BNNR:H) and (b) $N_a = 9$ (9-Ah-BNNR:H) are armchair ribbons having different width. N_a is the number of dimer lines across the ribbon width. (c)–(e) Zigzag ribbons of $N_z = 8$ (8-Zh-BNNR:H), $N_z = 9$ (9-Zh-BNNR:H), and $N_z = 7$ (7-Zh-BNNR), respectively. N_z is the number of zigzag chains across the ribbon width.

In this work, we study partially and fully screened Coulomb interaction parameters calculated with the *ab initio* cRPA and RPA methods [48–50], respectively. The fully screened Coulomb interaction W is related to the bare Coulomb interaction V as

$$W(\boldsymbol{r}, \boldsymbol{r}', \omega) = \int d\boldsymbol{r}'' \epsilon^{-1}(\boldsymbol{r}, \boldsymbol{r}'', \omega) V(\boldsymbol{r}'', \boldsymbol{r}'), \tag{1}$$

where $\epsilon(\boldsymbol{r}, \boldsymbol{r}'', \omega)$ is the dielectric function.

In the RPA of the dynamically screened Coulomb interaction, the dielectric function is related to the electron polarizability P by

$$\epsilon(\boldsymbol{r}, \boldsymbol{r}', \omega) = \delta(\boldsymbol{r} - \boldsymbol{r}') - \int d\boldsymbol{r}'' V(\boldsymbol{r}, \boldsymbol{r}'') P(\boldsymbol{r}'', \boldsymbol{r}', \omega), \tag{2}$$

where the polarization function $P(\boldsymbol{r}'', \boldsymbol{r}', \omega)$ is given by

$$P(\boldsymbol{r}, \boldsymbol{r}', \omega) = \sum_{\sigma} \sum_{\boldsymbol{k},m}^{occ} \sum_{\boldsymbol{k}',m'}^{unocc} \varphi^{\sigma}_{\boldsymbol{k}m}(\boldsymbol{r}) \varphi^{\sigma *}_{\boldsymbol{k}'m'}(\boldsymbol{r}) \varphi^{\sigma *}_{\boldsymbol{k}m}(\boldsymbol{r}') \varphi^{\sigma}_{\boldsymbol{k}'m'}(\boldsymbol{r}') \times \left[\frac{1}{\omega - \epsilon^{\sigma}_{\boldsymbol{k}'m'} - \epsilon^{\sigma}_{\boldsymbol{k}m} - i\eta} - \frac{1}{\omega + \epsilon^{\sigma}_{\boldsymbol{k}'m'} - \epsilon^{\sigma}_{\boldsymbol{k}m} - i\eta} \right]. \tag{3}$$

Here, $\epsilon^{\sigma}_{\boldsymbol{k}m}$ are single-particle Kohn-Sham eigenvalues obtained from DFT and η is a positive infinitesimal. Further,

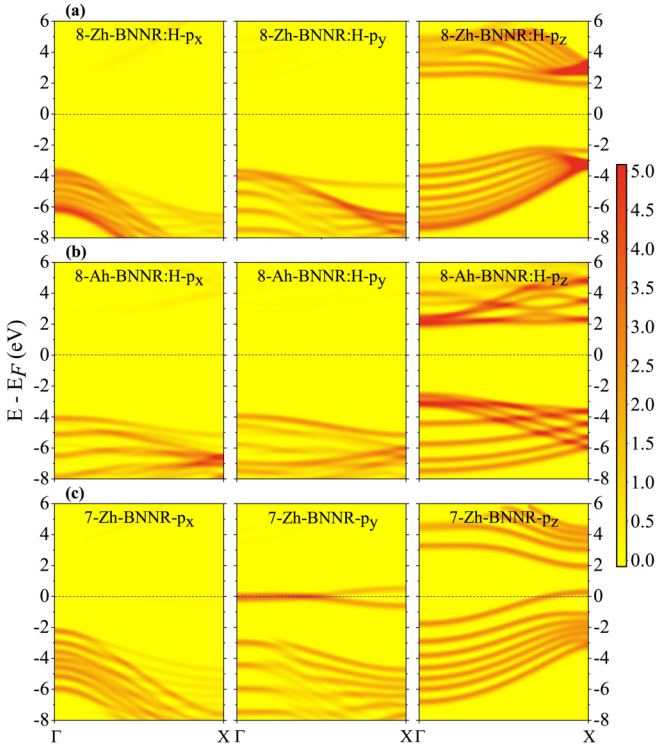

FIG. 2. Nonmagnetic orbital-projected band structure of (a) 8-Zh-BNNR:H, (b) 8-Ah-BNNR:H, and (c) 7-Zh-BNNR. The Fermi level is set to zero energy.

the $\varphi^{\sigma}_{km}(\boldsymbol{r})$ are the single-particle Kohn-Sham eigenstates with spin σ, wave number $\boldsymbol{k}$, and band index m. The tags *occ* and *unocc* above the summation symbol indicate that the summation is, respectively, over occupied and unoccupied states only.

In the cRPA, we separate the full polarization function into the two parts: P_l includes only transitions between the localized states, for which the interaction needs to be calculated, and P_r is the remainder,

$$P = P_l + P_r. \tag{4}$$

To identify the correlated subspace and understand which orbital should be considered in P_l, we need to look at the states near the Fermi energy for different nanoribbons. Projected band structures for two passivated systems, 8-Ah-BNNR:H and 8-Zh-BNNR:H, are depicted in Figs. 2(a) and 2(b), respectively. For both systems, the p_z orbitals have a significant contribution to the band around E_F compared to p_x and p_y orbitals and the corresponding p_z bands are disentangled from the rest in a large energy interval. In the case of nonpassivated nanoribbons [see Fig. 2(c) for 7-Zh-BNNR], all p_x, p_y, p_z, and s (not shown) orbitals are close to E_F. So, sp^3 orbitals must be considered as a correlated subspace.

The partially Coulomb interaction (Hubbard U) is written as

$$U(\omega) = [1 - VP_r(\omega)]^{-1}V. \tag{5}$$

Using maximally localized Wannier functions (MLWFs) at site R with orbital index n and spin σ, $w^{\sigma}_{Rn}(\boldsymbol{r})$, the matrix elements of the effective Coulomb potential U at frequency ω in the MLWFs basis are given by

$$U^{\sigma_1,\sigma_2}_{in_1,jn_3,in_2,jn_4}(\omega) = \iint d\boldsymbol{r}d\boldsymbol{r}' w^{\sigma_1 *}_{in_1}(\boldsymbol{r}) w^{\sigma_2 *}_{jn_3}(\boldsymbol{r}') U(\boldsymbol{r},\boldsymbol{r}',\omega) w^{\sigma_2}_{jn_4}(\boldsymbol{r}') w^{\sigma_1}_{in_2}(\boldsymbol{r}). \tag{6}$$

The average on-site interaction matrix elements of the effective Coulomb potential are estimated as [54]

$$U = 1/L \sum_n U^{\sigma_1,\sigma_2}_{Rnn:nn}(\omega = 0), \tag{7}$$

and off-site elements are defined as

$$U(R - R') = 1/L \sum_n U^{\sigma_1,\sigma_2}_{Rnn:R'nn}(\omega = 0), \tag{8}$$

where L is the number of localized orbitals. Using the WANNIER90 code [55], SPEX constructs MLWFs for the p orbitals of each atoms (10 states per atom) in all systems. We use $18 \times 18 \times 1$ and $30 \times 1 \times 1$ k-point grids in the cRPA calculations of the h-BN and h-BNNR unit cells, respectively. In Figs. 3(a) and 3(b), we have presented the original band structure and Wannier-interpolated bands obtained from the subspace selected by projecting onto p_z orbitals on each atom for 8-Ah-BNNR:H and sp^3 orbitals for 7-Zh-BNNR, respectively. The overall agreement between DFT-PBE and Wannier-interpolated bands is quite good and demonstrates the validity of the calculated Wannier functions.

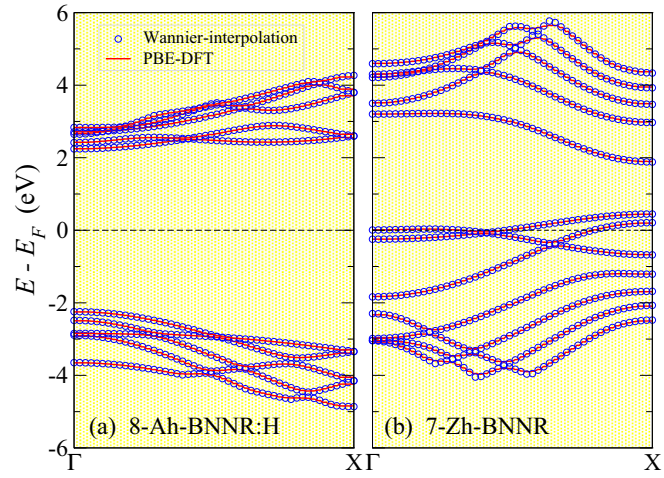

FIG. 3. DFT-PBE and Wannier-interpolated band structure of nonmagnetic (a) 8-Ah-BNNR:H and (b) 7-Zh-BNNR. Dashed lines denote the Fermi energy, which is set to zero.

III. RESULTS AND DISCUSSION

As shown in the band structure of Fig. 2, the passivated structures (8-Ah-BNNR:H and 8-Zh-BNNR:H) are semiconductors, while the bare zigzag nanoribbons (7-Zh-BNNR) are metallic. Since the electronic screening turns out to be strongly dependent on the band gap in the single-particle spectrum and dimensionality reduction, we present calculated values of Coulomb interaction parameters in three sections. In Sec. III A, we study the Coulomb interaction parameters

TABLE I. On-site (U_{00}), nearest-neighbor (U_{01}), next-nearest-neighbor (U_{02}), and third-nearest-neighbor (U_{03}) Coulomb interaction parameters (in eV) for 2D h-BN, 3D h-BN, and graphene. The bare V, partially screened (Hubbard U) (cRPA), and fully screened (W) (RPA) parameters are given. The values in the first and second rows of 2D h-BN and 3D h-BN for each Coulomb interaction parameter are related to N and B atoms, respectively.

	2D h-BN			3D h-BN			Graphene		
	Bare	cRPA	RPA	Bare	cRPA	RPA	Bare	cRPA	RPA
U_{00}	19.7	10.1	7.7	24.0	9.3	7.6	16.7	8.5	4.5
	15.0	8.7	6.7	19.6	8.7	7.5			
U_{01}	8.4	5.1	3.8	8.9	3.4	2.7	8.5	4.0	1.5
	8.4	5.1	3.8	8.9	3.4	2.7			
U_{02}	5.4	3.6	2.7	5.5	2.1	1.7	5.4	2.5	0.9
	5.2	3.5	2.7	5.4	2.0	1.7			
U_{03}	4.7	3.2	2.5	4.4	1.3	1.0	4.7	2.2	0.5
	4.7	3.2	2.5	4.4	1.3	1.0			

for 2D h-BN and three-dimensional bulk h-BN. In Sec. III B, we consider nonmetallic passivated nanoribbons with different widths with zigzag and armchair edge. In Sec. III C, we give the results for metallic nonpassivated nanoribbon (7-Zh-BNNR).

A. Two-dimensional h-BN and three-dimensional bulk h-BN

Considering Table I, we begin with the discussion of the bare V, partially U (cRPA), and fully W (RPA) Coulomb interaction parameters for 2D h-BN and 3D h-BN. The local (on-site U_{00}) and nonlocal (off-site U_{01}, U_{02}, and U_{03}) Coulomb matrix elements are also reported. Indexes of 00, 01, 02, and 03 are related to the strength of the potential that on-site, nearest-neighbor, next-nearest-neighbor, and third-nearest-neighbor parameters are feeling, respectively. For comparison, the corresponding results for pristine graphene are also presented. Due to two inequivalent sublattices of h-BN, the corresponding U values for B and N atoms are reported separately. Due to the existence of the band gap in 2D h-BN and 3D h-BN, the calculated on-site U values (Hubbard U) are larger than the corresponding values in graphene. In both sublattices of 2D h-BN, the screening is very weak and we obtain comparatively large U_{00} values of 10.1 and 8.7 eV for B and N atoms, respectively. The corresponding U_{00} values of 3D h-BN for B and N atoms are 9.3 and 8.7 eV, respectively, which shows that Hubbard U is about 1 eV smaller in the N sublattice. Moreover, the nonlocal U values in 2D h-BN are weakly screened and the calculated off-site U_{01}, U_{02}, and U_{03} parameters turn out to be rather sizable. In spite of the existence of the band gap in 3D h-BN, the off-site effective Coulomb interaction drops faster than graphene. It shows that Coulomb interaction of 2D h-BN is weakly screened at short distances, while it is almost unscreened at large distances. Screening of Coulomb interaction is closely related to the band gap of the materials. The GW approximation shows the 6 and 5.4 eV band gaps for 2D h-BN and 3D h-BN, respectively, which is significantly larger than the 4.5 and 5.0 eV band gap predicted by the GGA approximation [30,56,57]. Such remarkable many-body GW corrections to the band gap are attributed to the large Coulomb interactions.

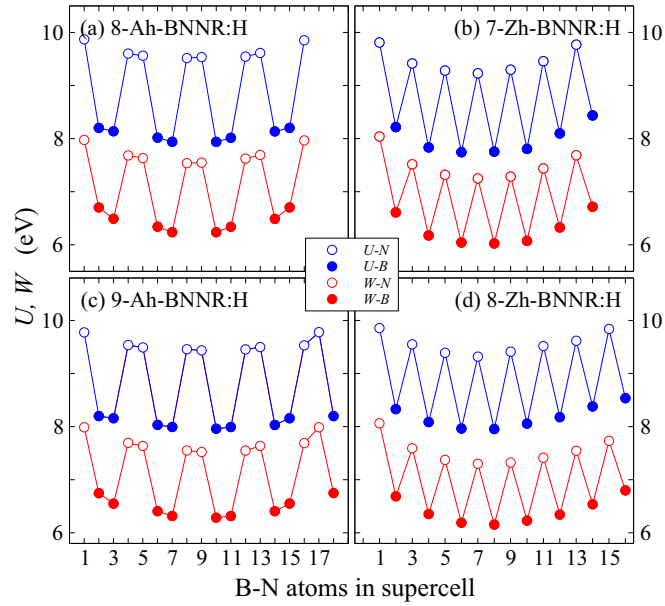

FIG. 4. Calculated partially screened on-site interaction U (blue line) and fully screened Coulomb interaction W (red line) of p_z electrons for (a) 8-Ah-BNNR:H, (b) 7-Zh-BNNR:H, (c) 9-Ah-BNNR:H, and (d) 8-Zh-BNNR:H.

B. Hydrogen-passivated nanoribbons: Armchair and zigzag edge

In the following, we show the changes in on-site effective Coulomb interaction (Hubbard U) and fully screened potential (W) across the passivated nanoribbon's unit cell in Fig. 4. We will consider systems having two different widths in each group, i.e., 8-Ah-BNNR:H and 9-Ah-BNNR:H with armchair edge and also 7-Zh-BNNR:H and 8-Zh-BNNR:H with zigzag edge. It can be observed that Coulomb parameters of h-BNNR:H are slightly smaller than the parameters for 2D h-BN (see Table I). For example, the obtained U (W) parameters vary in the range 7.9–10.0 eV (6.2–8.0 eV) for 8-Ah-BNNR:H. Similar to h-BN, the U and W parameters for the N atoms (unfilled points in Fig. 4) are about 2 eV larger than the corresponding ones for B atoms (filled points in Fig. 4) on the opposite sublattice. Moreover, for the inner atoms in the unit cell, we obtain a substantial reduction in the Coulomb interactions. This reduction in the Coulomb interaction is more pronounced for zigzag system 7-Zh-BNNR:H. The reduction in U and W for inner atoms and the difference of Coulomb parameters between the B and N atoms can be described by the atom-projected density of states (DOS) presented in Fig. 5. Since the p_z states of N atoms are occupied, their contribution to the polarization function is small. In other words, the B atoms has a large conduction p_z peak around E_F, while this peak is almost absent for N atoms. As a consequence, electronic screening increases significantly due to the contribution of the $\sigma \rightarrow p_z$ and $p_z \rightarrow p_z$ transition and, as a result, gives rise to smaller Coulomb interaction parameters for the B atoms.

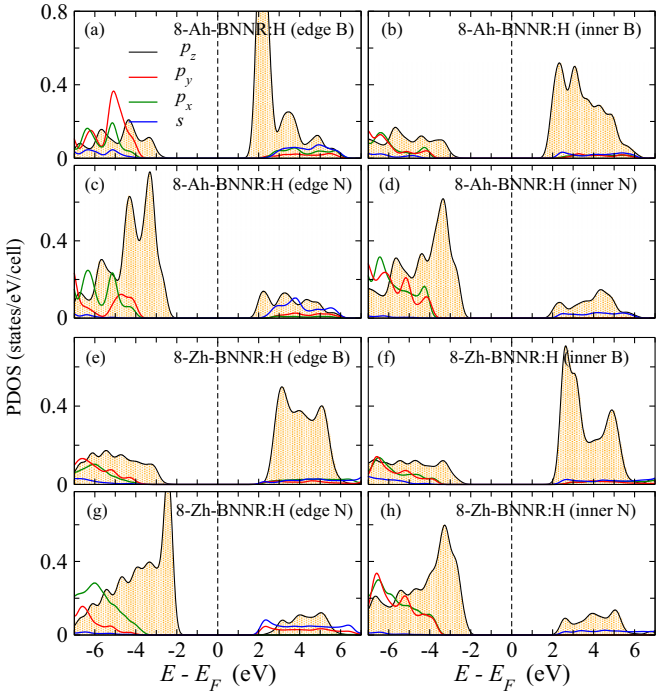

FIG. 5. Projected DOS for (a) edge B, (b) inner B, (c) edge N, and (d) inner N of 8-Ah-BNNR; and (e) edge B, (f) inner B, (g) edge N, and (h) inner N of 8-Zh-BNNR:H.

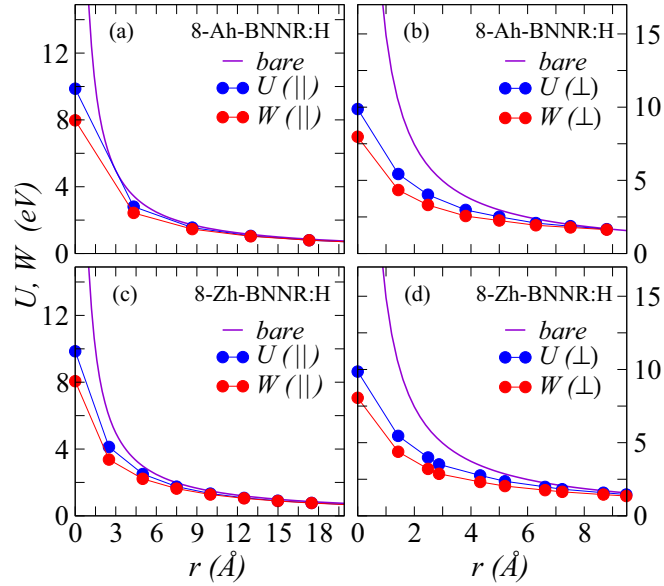

FIG. 6. Bare, partially, and fully screened Coulomb interaction for B-N p_z electrons as a function of distance r for (a), (b) 8-Ah-BNNR:H and (c),(d) 8-Zh-BNNR:H. Here, $U(\|)$ and $U(\perp)$ correspond to interactions along the ribbon and across the ribbon, respectively.

It is instructive to compare our results with the recent study of the GNRs. For example, considering the armchair GNRs (AGNRs) with the same width, 8-AGNR:H, the calculated $U(W)$ values turn out to be around 9.2 eV (5.5 eV), with very small variation from atom to atom [39]. These values are larger than the corresponding $U(W)$ ones for B atoms and smaller than for N atoms in 8-Ah-BNNR:H. In contrast to 8-Zh-BNNR:H showing a large band gap, the existence of edge states in GNRs with zigzag edges, 8-ZGNR:H, gives rise to a large contribution to the DOS exactly at E_F, and thus the on-site Coulomb interaction reduces to a small value of 5.1 eV at the edge. The $U - W$ differences in h-BNNR:H systems vary between 1.5 and 2.0 eV, while in GNR:H, the corresponding values are around 3.5–4.0 eV. A small contribution of the p_z states around E_F in both Ah-BNNR:H and Zh-BNNR:H systems results in the small screening through $p_z \rightarrow p_z$ transitions; as a consequence, $U - W$ differences become small for all atoms.

So far we have only considered the on-site Coulomb interactions in h-BNNR:H. In the following, we will discuss the intersite Coulomb interaction parameters for both h-BNNRs with armchair and zigzag edges. In Fig. 6, the bare V, partially U, and fully screened W average intersite Coulomb interactions as a function of distance r between two atoms for 8-Ah-BNNR:H and 8-Zh-BNNR:H are presented. The results along the ribbon $U(\|)$ $[W(\|)]$ and across the ribbon $U(\perp)$ $[W(\perp)]$ are shown separately. As shown in Fig. 6, Coulomb interaction is only screened at short distances and is more or less unscreened at long distances. Furthermore, the nonlocal Coulomb interaction $U(\perp)$ $[W(\perp)]$ is slightly larger than the $U(\|)$ $[W(\|)]$. Considering the central atoms in 8-Ah-BNNR:H, $V - W$ become negative at an intersite distance of 25 Å, indicating an antiscreening of Coulomb interactions in these quasi-one-dimensional systems. Moreover, antiscreening is not seen across the ribbon. Antiscreening means that the fully screened interaction W is larger than the bare interaction V. This behavior is consistent with the fact that the screening is nonconventional in low-dimensional systems, i.e., at short distances, the Coulomb interaction is weakly screened, while at middle distances, it is antiscreened, and, finally, it is unscreened at long distances.

In the case of 8-Ah-BNNR:H, antiscreening takes place between critical intersite distances $r_{c1} = 25$ Å and $r_{c2} = 74$ Å. The r_{c1} are the critical distances where the transition from screening to antiscreening occurs, and r_{c2} are the critical distances where the transition from antiscreening to unscreening takes place. Furthermore, moving from the central atoms in the nanoribbons to the edge atoms, the antiscreening weakens. In Fig. 7, we present the difference $V - W$ as a function of distance r between atoms along the ribbon for the edge and central atoms of 9-Ah-BNNR:H and 6-Zh-BNNR:H separately. It is noteworthy that the antiscreening phenomenon only occurs for central atoms along the ribbon. From now on, we can only consider the central atoms to evaluate the strength of antiscreening. To reveal the behavior of the Coulomb interaction at intermediate distance and the occurrence of antiscreening, we have extended the calculations to much wider nanoribbons, and we present the $V - W$ difference for $N_a = 2$ (2-Ah-BNNR:H) to $N_a = 11$ (11-Ah-BNNR:H) and $N_z = 3$ (3-Zh-BNNR:H) to $N_z = 9$ (9-Zh-BNNR:H) in Fig. 8. As expected, the antiscreening region $r_{c2} - r_{c1}$ and the negative values of $V - W$ tend to be reduced with increasing the ribbon width in both armchair and zigzag systems. For example, considering the smallest armchair nanoribbons

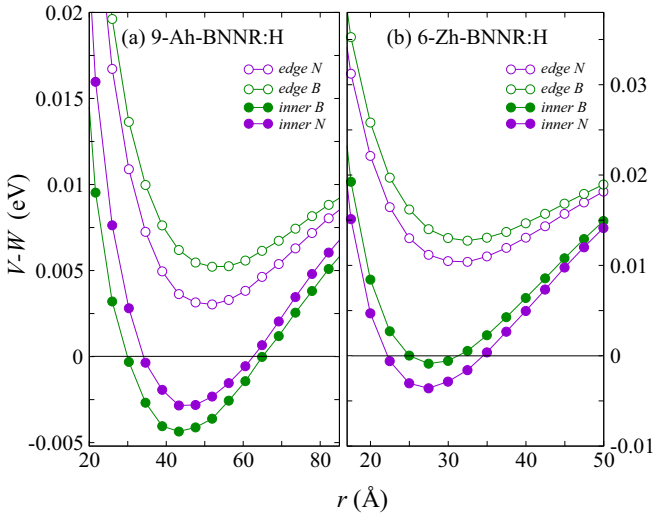

FIG. 7. The difference $V - W$ between bare interaction V and fully screened interaction W as a function of distance r between B-N atoms along the ribbon for the edge and central atoms of (a) 9-Ah-BNNR:H and (b) 6-Zh-BNNR:H.

2-Ah-BNNR:H, antiscreening is observed between intersite distance of $r_{c1} = 7.8$ Å and $r_{c2} = 92$ Å, but antiscreening is not observed in wider armchair nanoribbons 11-Ah-BNNR:H. There is no antiscreening with a width larger than 12.6 Å for both Ah-BNNR:H and Zh-BNNR:H. Consequently, there is a critical width such that if the nanoribbon width is larger than this threshold, the antiscreening effect is not observed.

The antiscreening discussed above was confirmed in one-dimensional semiconductors and large molecules [35,36]. Simply stated, if one electron is exposed to an electric field of another electron, the medium responds by rearranging the other charges in such a way as to weaken the bare interaction between the two electrons, which is called screening. Similarly, antiscreening occurs when the medium enhances the bare interaction between the two electrons. To understand how the antiscreening takes place, one can consider that the medium consists of point dipoles leaving around two point

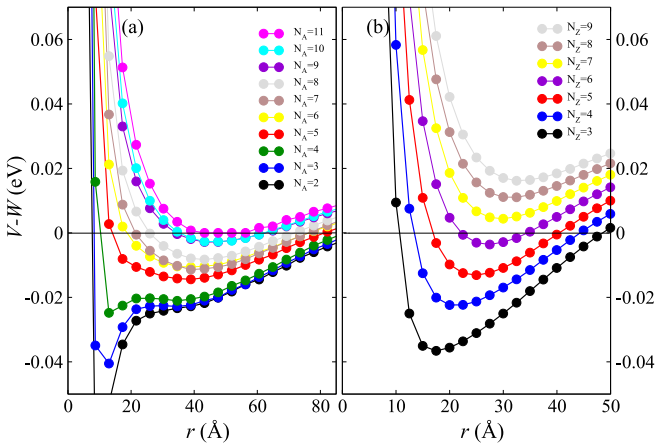

FIG. 8. The difference $V - W$ value as a function of distance r for central atoms of (a) $N_a = 2$ to $N_a = 11$ Ah-BNNR:H and (b) $N_z = 3$ to $N_z = 9$ Zh-BNNR:H.

TABLE II. The value of critical distances r_{c1} (transition from screening to antiscreening) and r_{c2} (transition from antiscreening to unscreening) in Å for different one-dimensional systems, zero-dimensional molecules, and clusters.

System	r_{c1}	r_{c2}	system	r_{c1}	r_{c2}
2-Ah-BNNR:H	7.8	92	6-AGNR [39]	22	115
3-Ah-BNNR:H	8.3	90	7-AGNR [39]	22	110
4-Ah-BNNR:H	10	88	8-AGNR [39]	35	105
5-Ah-BNNR:H	12.5	86	9-AGNR [39]	23	65
6-Ah-BNNR:H	17	85	CNT [36]	20	≈ 200
7-Ah-BNNR:H	21	78	C_{60} [58]	4.0	
8-Ah-BNNR:H	25	74	Fe_2O_3 [59]	2.45	
9-Ah-BNNR:H	28	68	Fe_3O_4 [59]	3.40	
3-Zh-BNNR:H	10.5	49	Fe_4O_6 [59]	2.90	
4-Zh-BNNR:H	13.5	45	Nb_4Co [60]	3.90	
5-Zh-BNNR:H	16.5	41	Naphtalene [35]	2.5	
6-Zh-BNNR:H	22	35	Benzene [35]	2.0	

charges. We can divide point dipoles into two groups: screening dipoles and antiscreening dipoles. Dipoles in the space between the charges result in enhancement, i.e., antiscreening, of the bare interaction, whereas the other surrounding dipoles reduce, i.e., screen, the bare interaction. For one-dimensional systems, the ratio of the antiscreening region (space between the charges) to the outside region is significant. That is why antiscreening occurs in one-dimensional systems such as carbon nanotubes, large organic molecules, and clusters [35,36,59,60].

As mentioned above, antiscreening is observed in several low-dimensional semiconductors and insulators. In order to compare our results with them, we present in Table II the antiscreening parameters r_{c1} and r_{c2} for all considered materials in the literature. The critical distance of antiscreening that we found for h-BNNR:H is longer than the zero-dimensional molecules $r_{c1} = 3 - 4$ Å [35], Fe_xO_y $r_{c1} = 2 - 3$ Å [59], and Nb_4Co $r_{c1} = 3.9$ Å [60], but slightly shorter than the corresponding ones for quasi-one-dimensional single-wall carbon nanotubes $r_{c1} = 20$ Å [35,36] and AGNR:H $r_{c1} = 20$–30 Å [39]. Even r_{c1} in the quasi-one-dimensional 2-Ah-BNNR:H is comparable to the Nb_4Co cluster.

In addition to geometry, the polarizability of the atoms constituting the system plays an important role in the antiscreening since atoms of the systems can be considered as a collection of point dipoles. The polarizability of atoms, which is inversely proportional to the energy difference between occupied and unoccupied states, reduces the magnitude of the antiscreening contribution and increases the onset of antiscreening r_{c1}. This describes the smaller critical distance r_{c1} and larger antiscreening contribution for h-BNNR:H compared to AGNR systems. The AGNR has more states around the E_F with respect to h-BNNR:H systems due to the small band gap. A similar discussion holds for a comparison of antiscreening for edge and inner atoms. As shown in Fig. 6, the antiscreening along the ribbon for edge atoms is weaker than the inner atoms and the critical distance of antiscreening r_{c1} at the edge is slightly longer. Then the antiscreening region $r_{c2} - r_{c1}$ is shorter at the edge, which is in good agreement with the behavior of our calculated band gaps.

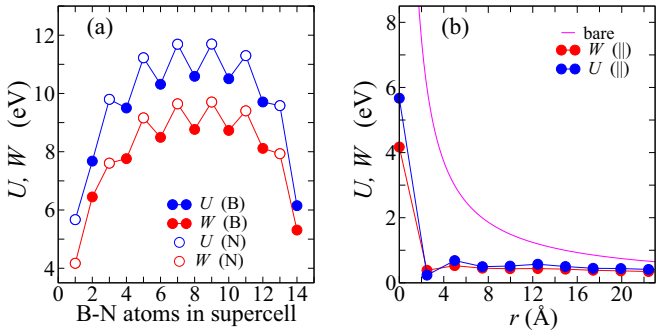

FIG. 9. (a) Hubbard U and fully screened interactions W for 7-Zh-BNNR. (b) Bare, partially U, and fully W screened off-site interactions as a function of distance r for 7-Zh-BNNR.

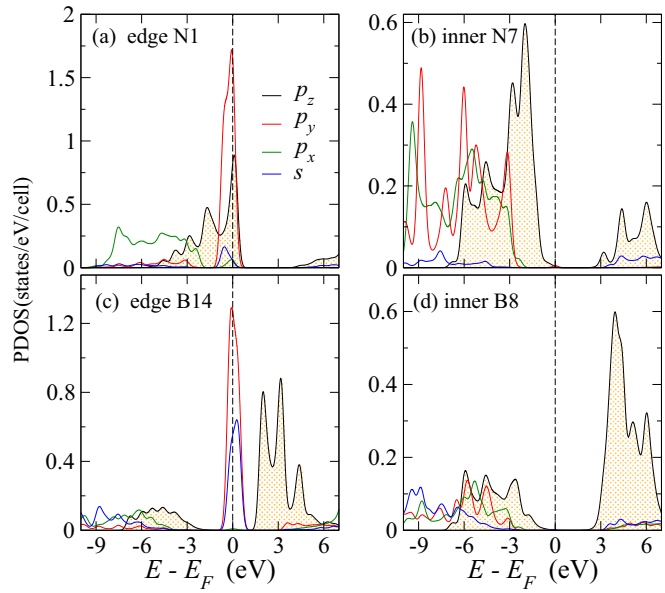

FIG. 10. Orbital-projected DOS for (a) edge N [atom number 1 in Fig. 1(e)], (b) inner N (atom number 7), (c) edge B (atom number 14), and (d) inner B (atom number 8) of 7-Zh-BNNR.

As we mentioned, for both armchair and zigzag h-BNNR:H, the screening is small and nonconventional. Due to this nonconventional screening, the calculated nonlocal interactions turn out to be extremely large. Tightly bound excitons are the consequence of this reduced dielectric screening of nonlocal Coulomb interactions for low-dimensional systems. Such an enhanced excitonic state with binding energy about 2.5 eV has been observed experimentally in the h-BNNR:H [32,33], which is in good agreement with *ab initio* calculations [32]. A similar strong excitonic state is observed in 2D semiconductor systems such as graphene [37], AGNR [34,41,42,45,61,62], fluorographene [63], phosphorene [64,65], and transition-metal dichalcogenides [66–71] such that these reduced dimensionality systems have a small dielectric screening of the Coulomb interaction.

C. Nonpassivated nanoribbons: Zigzag edge

In the following, we will discuss Coulomb interaction parameters for nonpassivated zigzag h-BNNR of $N_z = 7$ (7-Zh-BNNR). Nonpassivated armchair h-BNNRs (Ah-BNNRs) are semiconductors and their Coulomb interaction parameters are similar to passivated Ah-BNNRs:H. So we do not give the results for nonpassivated Ah-BNNRs. Bare h-BNNR with a zigzag edge are magnetic systems [24], but spin polarization has a weak influence on Coulomb interactions of zigzag systems about 0.2 eV. So, the on-site and off-site U and W values presented in Figs. 9(a) and 9(b) are for the non-spin-polarized case. Projected non-spin-polarized DOS for inner and edge atoms are also depicted in Fig. 10. Generally, due to the existence of metallic states around E_F, Coulomb interaction U and W tend to be reduced at the edge as compared to passivated nanoribbons. The U and W parameters for the atoms in the 7-Zh-BNNR show strong variations. This variation can be explained by the fact that as one moves from inner atoms to edge ones, the density of the p state of the corresponding atoms at E_F increases, which gives rise to the reduction of U and W parameters for edge atoms. Moreover, as seen in Fig. 10, the nonpassivated zigzag system exhibits more overlap of s, p_x, p_y, and p_z with respect to passivated systems. As a consequence, the correlated subspace is sp^3 in the nonpassivated zigzag h-BNRs. It can be found that the calculated U (W) values of inner N atoms of 7-Zh-BNNR turn out to be 11.6 eV (9.8 eV). Due to metallic states, Coulomb interaction is strongly screened for the edge N atoms and U reaches a relatively small value of 5.7 eV. Since sp^3 orbitals are considered as a correlated subspace, the contribution of the $sp^3 \rightarrow sp^3$ transition gives rise to an enhancement of the electronic polarization, and we find small Coulomb W values.

Now, we discuss the nonlocal screened Coulomb interaction presented in Fig. 9(b). The situation for the nonlocal interaction of nonpassivated 7-Zh-BNNR is different compared to passivated systems. As expected, the large DOS can give rise to a significant reduction of nonlocal Coulomb interaction even at short distance. Nonlocal screened Coulomb interaction of passivated systems preserves at long distance, but for bare zigzag nanoribbons, it is fully screened at short separation around 5 Å. In contrast to the passivated zigzag nanoribbons, the effective Coulomb interaction in 7-Zh-BNNR is predominantly local due to the sharp drop of U versus r, as shown in Fig. 9(b). Therefore, due to the short-range nature of Coulomb interaction, the zigzag system can be interpreted as a correlated material.

The edge states at E_F provide a metallic phase in the non-spin-polarized calculation and make the system unstable upon local electron-electron interaction to induce spin-polarized states. Experimental results show that spin-polarized states were observed in nonpassivated zigzag nanoribbons [19,27]. As we discussed above, the large DOS at the vicinity of E_F results in small long-range Coulomb interaction even at short distance. Hence, the on-site Hubbard term is sufficient to describe ferromagnetism in nonpassivated zigzag systems. Due to the Stoner criterion, $UD(E_F) > 1$ at edge atoms, and the nonpassivated system 7-Zh-BNNR therefore prefers the ferromagnetic ground state. The DOS at the Fermi energy $D(E_F)$, magnetic moments, and the Stoner criterion $UD(E_F)$ are presented in Table III for all atoms of the 7-Zh-BNNR system. Only atoms located at the edge of the ribbon satisfy the Stoner criterion $UD(E_F) > 1$ due to the large $D(E_F)$ at the

TABLE III. DOS at Fermi level E_F [$D(E_F)$], Stoner criterion $UD(E_F)$, and magnetic moment (MM) in μ_B for 7-Zh-BNNR nanoribbons.

Atom	$D(E_F)$ (1/eV)	$UD(E_F)$	MM (in μ_B)
N1	2.5867	**14.66**	−0.849
B2	0.0302	0.23	0.077
N3	0.5113	**5.01**	−0.130
B4	0.0219	0.21	0.009
N5	0.0688	0.77	−0.015
B6	0.0065	0.07	0.001
N7	0.0087	0.10	−0.002
B8	0.0030	0.03	0.001
N9	0.0028	0.03	−0.001
B10	0.0176	0.18	0.006
N11	0.0150	0.17	−0.002
B12	0.1799	**1.75**	0.061
N13	0.1020	0.97	−0.005
B14	1.8350	**11.28**	0.842

E_F and, as a result, the paramagnetic state is unstable towards the formation of ferromagnetism. Considering the zigzag graphene nanoribbons 8-ZGNR:H, the calculated magnetic moment turns out to be around 0.35 μ_B at the edge and it becomes rapidly destroyed towards the center of the ribbon [39]. The magnetic moment of edge atoms in 7-Zh-BNNR (0.85 μ_B) is much larger than that of the GNRs with zigzag edges. The calculated magnetism persists for atoms at the vicinity of the edge and disappears towards the center of the ribbon.

IV. CONCLUSION

We have studied the screening of the on-site and long-range Coulomb interactions for p electrons of pristine 2D h-BN, bare h-BNNRs, and passivated h-BNNRs by employing first-principles calculations in conjunction with the random-phase approximation. Screening strongly depends on the ribbon width, type of atoms (B or N), and the position of atoms in the unit cell. Our calculated Coulomb matrix elements considerably increase the predictive power of the model Hamiltonians applied to describe the electronic and magnetic properties of h-BN-based materials. We found sizable local U and W parameters for pristine 2D h-BN and passivated h-BNNRs with armchair edge and they are larger than the corresponding values in carbon-based materials. Reduced dimensionality and the presence of the band gap results in a decreased and nonconventional screening of the Coulomb interaction, i.e., Coulomb interaction is antiscreened at intermediate distances between 8 and 90 Å. This antiscreening becomes weaker as one moves from the center to the edge of passivated h-BNNRs. Sizable nonlocal parameters agree well with the strong excitonic effect observed in the experiments. The critical distance for the onset of antiscreening in h-BNNR is longer than in zero-dimensional molecules and clusters, but shorter than in GNRs and carbon nanotubes. Furthermore, the antiscreening effect disappears when the nanoribbon width is larger than the critical width 12.5 Å. For bare zigzag h-BNNR, we find that the interactions turn out to be local, and the nonlocal part is strongly screened due to the metallic states. The p states are very well screened, imposing a strong itinerant character of magnetism. We discuss the appearance of ferromagnetism in 7-Zh-BNNR using the Stoner model.

ACKNOWLEDGMENT

The authors acknowledge the computational resources provided by the Physics Department of Tarbiat Modarres University.

[1] A. K. Geim and K. S. Novoselov, Nat. Mater. **6**, 183 (2007).
[2] M. I. Katsnelson, Mater. Today **10**, 20 (2007).
[3] D. C. Elias, R. R. Nair, T. M. G. Mohiuddin, S. V. Morozov, P. Blake, M. P. Halsall, A. C. Ferrari, D. W. Boukhvalov, M. I. Katsnelson, A. K. Geim, and K. S. Novoselov, Science **323**, 610 (2009).
[4] J. Zhou, Q. Wang, Q. Sun, X. S. Chen, Y. Kawazoe, and P. Jena, Nano Lett. **9**, 3867 (2009).
[5] M. M. Ugeda, I. Brihuega, F. Guinea, and J. M. Gómez-Rodríguez, Phys. Rev. Lett. **104**, 096804 (2010).
[6] K. M. McCreary, A. G. Swartz, W. Han, J. Fabian, and R. K. Kawakami, Phys. Rev. Lett. **109**, 186604 (2012).
[7] R. R. Nair, M. Sepioni, I.-L. Tsai, O. Lehtinen, J. Keinonen, A. V. Krasheninnikov, T. Thomson, A. K. Geim, and I. V. Grigorieva, Nat. Phys. **8**, 199 (2012).
[8] G. Zsolt Magda, X. Jin, I. Hagymasi, P. Vancso, Z. Osvath, P. Nemes-Incze, C. Hwang, L. P. Biro, and L. Tapaszto, Nature (London) **514**, 608 (2014).
[9] X. Li, X. Wang, L. Zhang, S. Lee, and H. Dai, Science **319**, 1229 (2008).
[10] L. Xian, D. M. Kennes, N. Tancogne-Dejean, M. Altarelli, and A. Rubio, Nano Lett. **19**, 4934 (2019).
[11] L. Sponza, H. Amara, F. Ducastelle, A. Loiseau, and C. Attaccalite, Phys. Rev. B **97**, 075121 (2018).
[12] G. Cassabois, P. Valvin, and B. Gil, Nat. Photon. **10**, 262 (2016).
[13] R. Bourrellier, M. Amato, L. H. Galvão Tizei, C. Giorgetti, A. Gloter, M. I. Heggie, K. March, O. Stéphan, L. Reining, M. Kociak, and A. Zobelli, ACS Photon. **1**, 857 (2014).
[14] Y. Kubota, K. Watanabe, O. Tsuda, and T. Taniguchi, Science **317**, 932 (2007).
[15] C. R. Dean, A. F. Young, I. Meric, C. Lee, L. Wang, S. Sorgenfrei, K. Watanabe, T. Taniguchi, P. Kim, K. L. Shepard, and J. Hone, Nat. Nanotechnol. **5**, 722 (2010).
[16] K. Watanabe, T. Taniguchi, and H. Kanda, Nat. Mater. **3**, 404 (2004).
[17] A. Nagashima, N. Tejima, Y. Gamou, T. Kawai, and C. Oshima, Phys. Rev. Lett. **75**, 3918 (1995).
[18] J. D. Caldwell, A. V. Kretinin, Y. Chen, V. Giannini, M. M. Fogler, Y. Francescato, C. T. Ellis, J. G. Tischler, C. R. Woods, A. J. Giles, and M. Hong, Nat. Commun. **5**, 5221 (2014).
[19] C. Jin, F. Lin, K. Suenaga, and S. Iijima, Phys. Rev. Lett. **102**, 195505 (2009).

[20] K. K. Kim, A. Hsu, X. Jia, S. M. Kim, Y. Shi, M. Hofmann, D. Nezich, J. F. Rodriguez-Nieva, M. Dresselhaus, T. Palacios, and J. Kong, Nano Lett. **12**, 161 (2011).

[21] G. Lu, T. Wu, Q. Yuan, H. Wang, H. Wang, F. Ding, X. Xie, and M. Jiang, Nat. Commun. **6**, 6160 (2015).

[22] B. Arnaud, S. Lebègue, P. Rabiller, and M. Alouani, Phys. Rev. Lett. **96**, 026402 (2006).

[23] M. Bernardi, M. Palummo, and J. C. Grossman, Phys. Rev. Lett. **108**, 226805 (2012).

[24] V. Barone and J. E. Peralta, Nano Lett. **8**, 2210 (2008).

[25] Z. Zhang and W. Guo, Phys. Rev. B **77**, 075403 (2008).

[26] H. Zeng, C. Zhi, Z. Zhang, X. Wei, X. Wang, W. Guo, Y. Bando, and D. Golberg, Nano Lett. **10**, 5049 (2010).

[27] M. Terrones, J.-C. Charlier, A. Gloter, E. Cruz-Silva, E. Terrés, Y. B. Li, A. Vinu, Z. Zanolli, J. M. Dominguez, H. Terrones, Y. Bando, and D. Golberg, Nano Lett. **8**, 1026 (2008).

[28] M. Topsakal, E. Aktürk, and S. Ciraci, Phys. Rev. B **79**, 115442 (2009).

[29] L. Museur and A. Kanaev, J. Appl. Phys. **103**, 103520 (2008).

[30] F. Ferreira, A. J. Chaves, N. M. R. Peres, and R. M. Ribeiro, J. Opt. Soc. Am. B **36**, 674 (2019).

[31] C. Hu, R. Ogura, N. Onoda, S. Konabe, and K. Watanabe, Phys. Rev. B **85**, 245420 (2012).

[32] S. Wang, Q. Chen, and J. Wang, Appl. Phys. Lett. **99**, 063114 (2011).

[33] Z. G. Chen, J. Zou, G. Liu, F. Li, Y. Wang, L. Wang, X. L. Yuan, T. Sekiguchi, H. M. Cheng, and G. Q. Lu, ACS Nano **2**, 2183 (2008).

[34] R. Denk, M. Hohage, P. Zeppenfeld, J. Cai, C. A. Pignedoli, H. Sode, R. Fasel, X. Feng, K. Mullen, S. Wang, D. Prezzi, A. Ferretti, A. Ruini, E. Molinari, and P. Ruffieux, Nat. Commun. **5**, 4253 (2014).

[35] J. van den Brink and G. A. Sawatzky, Europhys. Lett. **50**, 447 (2000).

[36] J. Deslippe, M. Dipoppa, D. Prendergast, M. V. O. Moutinho, R. B. Capaz, and S. G. Louie, Nano Lett. **9**, 1330 (2009).

[37] P. Cudazzo, I. V. Tokatly, and A. Rubio, Phys. Rev. B **84**, 085406 (2011).

[38] M. van Schilfgaarde and M. I. Katsnelson, Phys. Rev. B **83**, 081409(R) (2011).

[39] H. Hadipour, E. Şaşioğlu, F. Bagherpour, C. Friedrich, S. Blugel, and I. Mertig, Phys. Rev. B **98**, 205123 (2018).

[40] T. O. Wehling, E. Şaşıoğlu, C. Friedrich, A. I. Lichtenstein, M. I. Katsnelson, and S. Blugel, Phys. Rev. Lett. **106**, 236805 (2011).

[41] D. Prezzi, D. Varsano, A. Ruini, A. Marini, and E. Molinari, Phys. Rev. B **77**, 041404(R) (2008).

[42] D. Prezzi, D. Varsano, A. Ruini, and E. Molinari, Phys. Rev. B **84**, 041401(R) (2011).

[43] S. Wang and J. Wang, J. Phys. Chem. C **116**, 10193 (2012).

[44] C. Bronner, D. Gerbert, A. Broska, and P. Tegeder, J. Phys. Chem. C **120**, 26168 (2016).

[45] G. Soavi, S. D. Conte, C. Manzoni, D. Viola, A. Narita, Y. Hu, X. Feng, U. Hohenester, E. Molinari, D. Prezzi, K. Mullen, and G. Cerullo, Nat. Commun. **7**, 11010 (2016).

[46] E. Şaşioğlu, H. Hadipour, C. Friedrich, S. Blügel, and I. Mertig, Phys. Rev. B **95**, 060408(R) (2017).

[47] H. Hadipour, Phys. Rev. B **99**, 075102 (2019).

[48] F. Aryasetiawan, M. Imada, A. Georges, G. Kotliar, S. Biermann, and A. I. Lichtenstein, Phys. Rev. B **70**, 195104 (2004); F. Aryasetiawan, K. Karlsson, O. Jepsen, and U. Schonberger, *ibid.* **74**, 125106 (2006); T. Miyake, F. Aryasetiawan, and M. Imada, *ibid.* **80**, 155134 (2009).

[49] E. Şaşioğlu, C. Friedrich, and S. Blügel, Phys. Rev. B **83**, 121101(R) (2011); Phys. Rev. Lett. **109**, 146401 (2012).

[50] Y. Nomura, M. Kaltak, K. Nakamura, C. Taranto, S. Sakai, A. Toschi, R. Arita, K. Held, G. Kresse, and M. Imada, Phys. Rev. B **86**, 085117 (2012); B-C. Shih, Y. Zhang, W. Zhang, and P. Zhang, *ibid.* **85**, 045132 (2012).

[51] Available from: http://www.flapw.de/site/ (unpublished).

[52] J. P. Perdew, K. Burke, and M. Ernzerhof, Phys. Rev. Lett. **77**, 3865 (1996).

[53] C. Friedrich, S. Blügel, and A. Schindlmayr, Phys. Rev. B **81**, 125102 (2010).

[54] J. Hubbard, Proc. R. Soc. London A **276**, 238 (1963); J. Kanamori, Prog. Theor. Phys. **30**, 275 (1963); M. C. Gutzwiller, Phys. Rev. Lett. **10**, 159 (1963); V. I. Anisimov, I. V. Solovyev, M. A. Korotin, M. T. Czyzyk, and G. A. Sawatzky, Phys. Rev. B **48**, 16929 (1993); L. Vaugier, H. Jiang, and S. Biermann, *ibid.* **86**, 165105 (2012).

[55] A. A. Mostofi, J. R. Yates, Y.-S. Lee, I. Souza, D. Vanderbilt, and N. Marzari, Comput. Phys. Commun. **178**, 685 (2008); F. Freimuth, Y. Mokrousov, D. Wortmann, S. Heinze, and Blügel, Phys. Rev. B **78**, 035120 (2008).

[56] X. Blase, A. Rubio, S. G. Louie, and M. L. Cohen, Phys. Rev. B **51**, 6868 (1995).

[57] M. Kolos and F. Karlicky, Phys. Chem. Chem. Phys. **21**, 3999 (2019).

[58] J. Van den Brink and G. A. Sawatzky, AIP Conf. Proc. **442**, 152 (1998).

[59] L. Peters, E. Şaşıoğlu, S. Rossen, C. Friedrich, S. Blugel, and M. I. Katsnelson, Phys. Rev. B **95**, 155119 (2017).

[60] L. Peters, E. Şaşıoğlu, I. Mertig, and M. I. Katsnelson, Phys. Rev. B **97**, 045121 (2018).

[61] X. Zhu and H. Su, J. Phys. Chem. A **115**, 11998 (2011).

[62] L. Yang, M. L. Cohen, and S. G. Louie, Nano Lett. **7**, 3112 (2007).

[63] F. Karlicky and M. Otyepka, J. Chem. Theory Comput. **9**, 4155 (2013).

[64] J. Yang, R. Xu, J. Pei, Y. W. Myint, F. Wang, Zh. Wang, Sh. Zhang, Z. Yu, and Y. Lu, Light Sci. Appl. **4**, e312 (2015).

[65] Z. Nourbakhsh and R. Asgari, Phys. Rev. B **94**, 035437 (2016).

[66] A. Chernikov, T. C. Berkelbach, H. M. Hill, A. Rigosi, Y. Li, O. B. Aslan, D. R. Reichman, M. S. Hybertsen, and T. F. Heinz, Phys. Rev. Lett. **113**, 076802 (2014).

[67] K. He, N. Kumar, L. Zhao, Z. Wang, K. F. Mak, H. Zhao, and J. Shan, Phys. Rev. Lett. **113**, 026803 (2014).

[68] M. M. Ugeda, A. J. Bradley, S.-F. Shi, F. H. da Jornada, Y. Zhang, D. Y. Qiu, W. Ruan, S.-K. Mo, Z. Hussain, Z.-X. Shen, F. Wang, S. G. Louie, and M. F. Crommie, Nat. Mater. **13**, 1091 (2014).

[69] H. Shi, H. Pan, Y.-W. Zhang, and B. I. Yakobson, Phys. Rev. B **87**, 155304 (2013).

[70] D. Y. Qiu, F. H. da Jornada, and S. G. Louie, Phys. Rev. Lett. **111**, 216805 (2013).

[71] G. Berghäuser and E. Malic, Phys. Rev. B **89**, 125309 (2014).